ACS Energy LETTERS

http://pubs.acs.org/journal/aelccp

Benzo[c]cinnoline Organic Anode Enables 1.3 V-Class Alkaline Aqueous Batteries

Christopher Walter,[‡] Jaehyun Park,[‡] Edgar U. Lopez-Torres, Mark Yaseen, and Shiyu Zhang*

Cite This: *ACS Energy Lett.* 2025, 10, 629−634

Read Online

ACCESS | Metrics & More | Article Recommendations | Supporting Information

ABSTRACT: Benzo[c]cinnoline (**1**) is investigated as a low-potential organic anode material for alkaline aqueous batteries (AABs). As organic materials are typically poor catalysts for hydrogen evolution reaction (HER), anode prepared with **1** can significantly reduce the rate of hydrogen production and self-discharge, common issue with conventional metal hydride anodes. Galvanostatic charge−discharge tests of **1** paired with a $Ni(OH)_2$ cathode in an alkaline aqueous electrolyte (4 M KOH + 2 M KF + 2 M K_2CO_3) show a cell voltage of 1.3 V and a capacity of 229 mAh g^{-1}, with negligible capacity fading after 1000 cycles. The full cell, with a high loading of 11.1 mg cm^{-2}, delivers a specific energy of 67 Wh kg^{-1} (including both the anode and cathode masses). Furthermore, the electrode of **1** can be produced from the low-cost precursor 2,2′-dinitrobiphenyl (**2**, $1.64/g) via in situ electrochemical reduction, enhancing its potential for large-scale implementation.

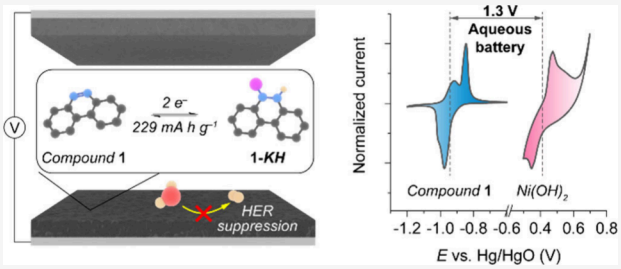

Aqueous batteries are an attractive energy media for applications with lower energy density requirements, such as grid-scale storage, wearable electronics, etc. They offer safer alternatives to lithium-ion batteries, which rely on flammable organic electrolytes.[1,2] Most common alkaline aqueous batteries (AABs) utilize metal-based anode materials,[3−6] which face several challenges, including a heavy reliance on metal mining, limited availability of raw materials,[7] and the promotion of the hydrogen evolution reaction (HER), which accelerates self-discharge and raises safety concerns.[8,9]

These disadvantages of inorganic anodes can be addressed by developing organic anode materials. First, organic electrode materials (OEMs) are more sustainable, as they are derived from abundant elements, such as C, H, N, O, and S.[10−12] Furthermore, organic materials typically are poor catalysts for HER with high overpotentials, potentially allowing the electrode to operate outside the narrow electrochemical stability window of aqueous electrolytes (1.23 V).[13] Currently, most of the development of OEMs focuses on cathode applications,[3,14−17] and the potential of organic anode materials in an aqueous environment has not been fully explored.[18−23]

Herein, we report the use of benzo[c]cinnoline (**1**) as a low potential (−0.927 to −0.997 V vs Hg/HgO) and high-capacity (244 mAh g^{-1}) organic anode material for alkaline battery applications. Electrodes prepared with **1** undergo stepwise potassium- and proton-coinsertion to form the potassium salt of dihydrobenzo[c]cinnoline (**1−KH**) as the discharged material. A proof-of-concept two-electrode cell assembled with **1** as the anode at a high loading of 11.1 mg cm^{-2} with a $Ni(OH)_2$ cathode shows a high cell voltage of 1.3 V and a specific energy of 67 Wh kg^{-1} (total mass of anode and cathode) (Figure 1A and 1B). Importantly, the organic anodes prepared with **1** exhibit a wider electrochemical stability window than conventional metal-hydride anodes, potentially avoiding the issues of hydrogen evolution and self-discharging and highlighting the advantage of organic electrode materials for aqueous batteries.

Prior to our work, the electrochemical behavior of **1** has only been briefly investigated with CV in the presence of a proton donor.[24−27] It was reported that benzo[c]cinnoline can undergo a two-electron two-proton reduction to dihydrobenzo[c]cinnoline (**1-H_2**). However, the reversibility of this redox process is unknown. To evaluate the viability of **1** as anode material for AABs, we performed galvanostatic charge−discharge (GCD) experiments in a three-electrode cell with a standard alkaline aqueous electrolyte (4 M KOH + 2 M K_2CO_3 + 2 M KF) and Hg/HgO reference electrode.

The solid-state CV of **1** shows two consecutive reduction events at −0.932 V and −0.968 V (Figure 1B). On the return sweep, two separate oxidation events at −0.957 V and −0.884

Received: November 7, 2024
Revised: December 13, 2024
Accepted: December 26, 2024
Published: January 3, 2025

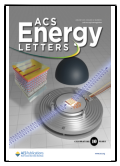

https://doi.org/10.1021/acsenergylett.4c03087
ACS Energy Lett. 2025, 10, 629−634

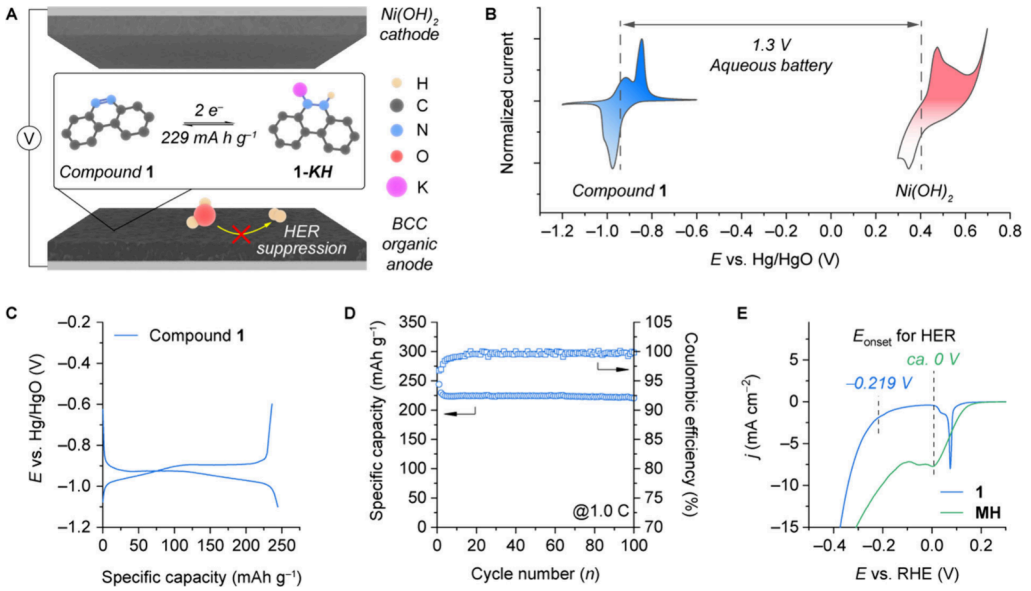

Figure 1. Electrochemical performance of compound 1. (A) Schematic illustration of compound 1/$Ni(OH)_2$ full cell structure. (B) CV profiles of compound 1 (blue) and $Ni(OH)_2$ (red) with proposed 1.3 V full cell voltage. (C) GCD and (D) cycling stability profile of compound 1 at 1C (1C = 297 mAh g^{-1}) in a three-electrode cell. (E) Determining the HER onset potentials of 1 (blue trace) vs conventional MH electrode (green trace).

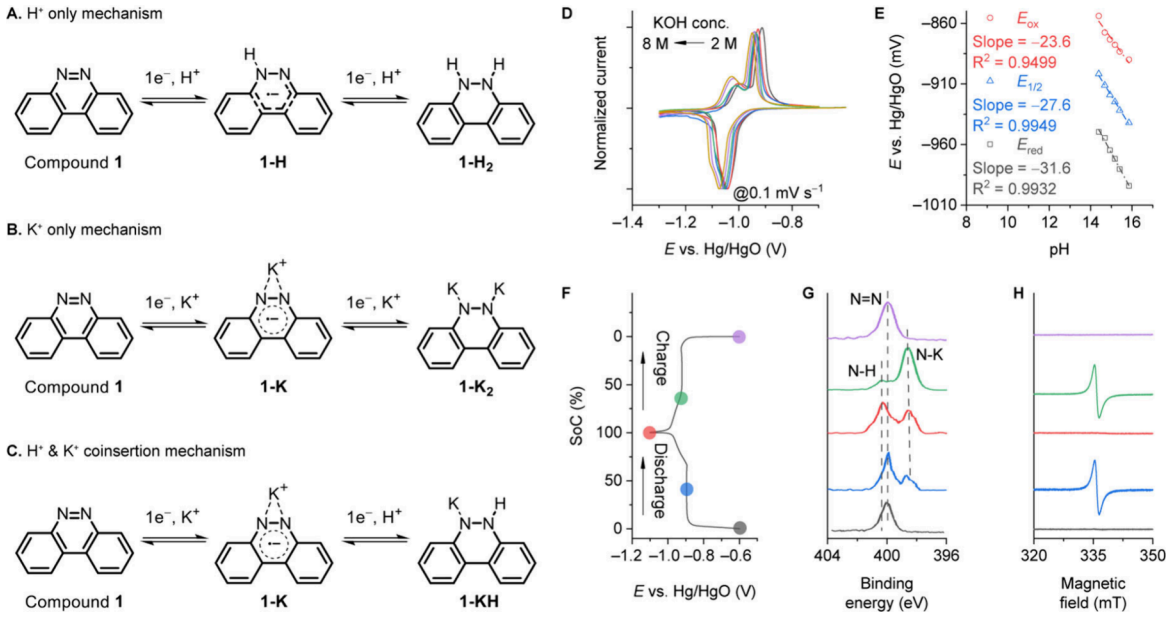

Figure 2. (A-C) Three proposed mechanisms for the redox of 1 in aqueous environment. (D) Solid-state CV of compound 1 in 2−8 M KOH as electrolyte. (E) *E*/pH dependence of compound 1 with the average reduction potentials (E_{red}) indicated as black, $E_{1/2}$ as blue, and average oxidation potentials (E_{ox}) as red, respectively. (F) GCD profile of compound 1 and corresponding (G) XPS and (H) EPR analysis of pristine (black), 40% reduced (blue), 100% reduced (red), 40% oxidized (green), and 100% oxidized (purple), respectively.

V occur. The power law fitting of the first redox event gives a *b* value of 0.50−0.59, and the second redox event gives a *b* value of 0.99−1.00 (Figure S3B). The difference in the *b* values suggests different ion insertion mechanisms, which will be further explored in the mechanistic investigation section.[28,29] The low redox potential of compound **1** makes it a promising candidate as an anode material for AABs, particularly when paired with a conventional $Ni(OH)_2$ cathode, yielding a full-cell voltage of ca. 1.3 V (Figure 1B).

The GCD of **1** at a rate of 1C (assuming two-electron redox processes, 297 mA g^{-1}) exhibits a discharge capacity of 244 mAh g^{-1}, representing 82% of the theoretical value (Figure 1C). The discharge curve initially shows a plateau at −0.927 V vs Hg/HgO, which gradually changes into a slope from −0.927 V to −0.997 V. During the charge, a slope from −0.998 V to −0.895 V occurs first, followed by a plateau at −0.895 V. Over 100 cycles, the GCD curve maintains a stable capacity of 220 mAh g^{-1} (Figure 1D).

Next, we investigated the electrochemical window of organic electrodes prepared with **1**. Organic materials are poor catalysts for HER, making **1** a potential solution to the hydrogen production and self-discharge issues associated with

https://doi.org/10.1021/acsenergylett.4c03087
ACS Energy Lett. 2025, 10, 629−634

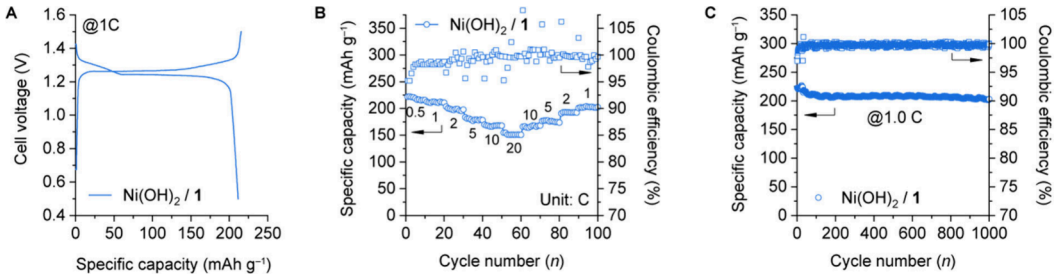

Figure 3. Electrochemical performance of a full cell with $Ni(OH)_2$ as cathode and compound 1 as anode with a 1.0 mg cm^{-2} loading in a standard ANAB electrolyte. (A) GCD at 1C (1C = 297 mAh g^{-1}), (B) rate capabilities 1 at various C rates, and (C) long-term cycling stability at 1C.

metal-hydride anodes. The reduced hydrogen generation could also enhance the safety of aqueous batteries, eliminating the need for additional mechanical controls to mitigate gas build-up, a common problem in metal hydride systems (Figure S4).[30−32]

Upon expansion of the CV scan window, we observed an onset HER potential of −0.219 V vs RHE (Figure 1E, blue trace). This value is much lower than the onset HER potential of metal hydride electrodes (0 V vs RHE, Figure 1E, green trace).[33,34] The redox of **1** occurs at a potential well above the HER onset potential (as indicated by the sharp anodic peak shape), effectively inhibiting HER production. In contrast, the redox of the metal hydride electrode has a significant overlap with HER, leading to hydrogen gas build-up and self-discharge issues commonly observed in metal hydride batteries. The metal hydride electrode was harvested from a commercial alkaline battery due to its well-established performance. The slowed HER during the redox of **1** is expected to benefit the stability and safety operation of AABs.

There are three plausible redox mechanisms of **1**. The first involves the reduction of **1** to form the two-electron two-proton product **1−H$_2$** (Figure 2A). Alternatively, potassium ions can serve as the charge carrier, inserting into **1** during reduction to form **1−K$_2$** (Figure 2B). This pathway is favored when the single and doubly reduced forms of **1** have a lower pK_a than the pH of the electrolyte (15.7). The third possible mechanism involves a mixed potassium and proton coinsertion process, where the initial reduction forms **1−K** and the second reduction leads to **1−KH** (Figure 2C). Determination of the electrochemical behavior of **1** under a basic environment offers insights into the interplay between proton-couple electron transfer (PCET) and potassium insertion, shedding light on the redox mechanisms of organic electrode materials in alkaline aqueous electrolytes.

First, we set out to determine the dependence of the redox potential on pH. Solid-state CV of **1** with varying concentrations of KOH (pH from 14.39 to 15.40)[35] reveals that the $E_{1/2}$ of **1** varies by 28 mV/pH unit, suggesting an overall two-electron one-proton PCET process (Figure 2D,E).[20,21,36] We propose that the additional negative charge introduced by the reduction is compensated by K^+ insertion. This hypothesis is probed by measuring the CV of **1** in a Li^+-based electrolyte (Figure S5). In 2 M LiOH, the reduction of **1** occurs at 37 mV more cathodic than 2 M KOH, and the reduction feature is significantly broader, suggesting a cation dependence impacting the reaction product.

Next, we probed the discharge product as a function of the state of charge of compound **1** (Figure 2F). The characterization of the reduction product **1** is difficult due to air-sensitivity. **1−H$_2$** is reported to rapidly react with O_2[37] and water[38] to regenerate **1**. Nonetheless, we evaluate the potential for ex-situ characterization by assessing the stability of the reduced product (Table S1). Fortunately, when the fully discharged electrode is dried under a stream of nitrogen, the resulting samples are stable enough for solid-state characterization with X-ray photoelectron spectrum (XPS) and electron paramagnetic resonance (EPR).

XPS analysis of **1** in the pristine state showed an N 1s signal at 399.9 eV with a full-width half max (fwhm) of 1.02 eV, consistent with N═N (Figure 2G, black trace).[39] Upon 40% reduction of **1** in a three-electrode cell, a broad shoulder feature at 398.0 eV appears (Figure 2G, blue trace), which was attributed to the N−K motif from **1−K**.[19,21] Upon full reduction (100%), the intensity of the N−K feature increases, accompanied by further broadening of the peak at 399.9 eV, indicating N−H bond formation (Figure 2G, red trace). A similar broadened N−H signal has been observed in pyrrolic nitrogen in pyrazoles.[40,41] When **1** is 40% oxidized, the N−H signal from **1−KH** at 399.9 eV diminishes in intensity compared to the N−K signal at 398.0 eV (Figure 2G, green trace). Upon full oxidation (100%), both the N−K and N−H signals disappear, and the original N═N signal of **1** is restored (Figure 2G, purple trace).

The EPR analysis further supports the assignment of a stepwise potassium-insertion and proton-insertion mechanism (Figure 2H). In the pristine state, **1** is EPR silent. Upon 40% reduction, a free radical signal at g = 2.002 emerges, consistent with previously reported solution EPR spectra of **1−K** derivatives (Figure 2H, blue trace).[42] At the fully reduced state (100%), the EPR spectrum returns to silent. When 1 is 40% oxidized, the free radical signal at g = 2.002 reappears (Figure 2H, green trace), but once fully oxidized, the spectrum becomes silent again. Taking the XPS and EPR together, **1** likely goes through a potassium- and proton-coinsertion mechanism (Figure 2C). The first reduction proceeds with K^+ insertion to form **1−K**, and the second reduction converts **1−K** to **1−KH**.

After establishing the redox mechanisms of **1** with three-electrode cells, we evaluated their cycling performance in two-electrode coin cells, which are more common in practical applications (Figure 3A). The weight percentage of the active materials was increased from 50% to 70% to achieve higher active material loading. Additionally, the electrodes were fabricated using a stainless-steel current collector instead of stainless-steel mesh. $Ni(OH)_2$ is used as the cathode in an excess mass anode: cathode ratio to assess the performance of the anode materials without interference from the $Ni(OH)_2$.

https://doi.org/10.1021/acsenergylett.4c03087
ACS Energy Lett. 2025, 10, 629−634

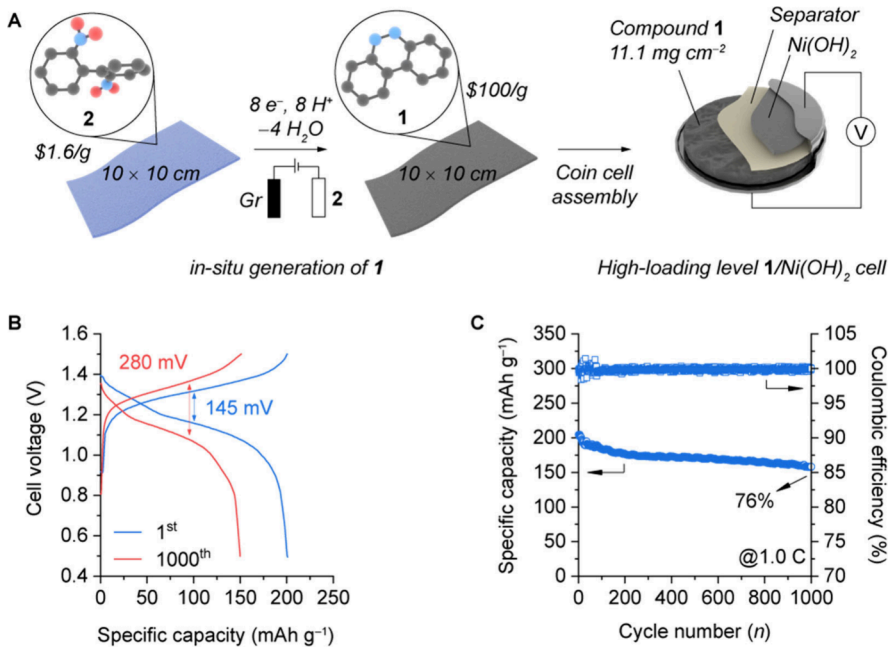

Figure 4. (A) In-situ electrochemical reduction mechanism of 2 to form 1, (B) GCD profile of full cell with a high areal loading of 1 at 11.1 mg cm^{-2}. The electrode of 1 in situ generated the electrochemical reduction of 2. The first GCD cycle after the formation of 1 from 2 is shown in blue, and 1000th cycle is shown in red. (C) Long-term cycling stability of the full cell at a rate of 3,296 mA (1 C).

The rate capability of **1** was evaluated at 0.5C, 1C, 2C, 5C, 10C, and 20C (ca. 6 A g^{-1}), showing capacities of 222 mAh g^{-1}, 211 mAh g^{-1}, 199 mAh g^{-1}, 180 mAh g^{-1}, 167 mAh g^{-1}, and 150 mAh g^{-1} respectively (Figure 3B). The voltage hysteresis remains low at 20 mV for 0.5C and increases slightly to 85 mV at 20C (Figure S11). Long-term cycling study at 1C shows excellent performance, with 90% capacity retention over 1000 cycles and an average Coulombic efficiency (CE) of 99.7% (Figure 3C).

A potential obstacle to deploying **1** as an OEM is its high cost, exceeding $100/g. This expense likely stems from its synthesis, which involves reducing 2,2′-dinitrobiphenyl (**2**) using palladium or indium catalysts.[43−45] However, if the reduction of the inexpensive precursor **2** ($1.64/g) to **1** could be integrated into the electrode fabrication process, it would significantly lower production costs and accelerate the commercial viability of **1**.[46−48]

To address this issue, we examined whether **1** could be produced in situ from the electrochemical reduction of electrodes containing **2**. Electrodes with a 70% loading of **2** were fabricated and assembled in a two-electrode coin cell with a Ni(OH)$_2$ cathode and a standard alkaline electrolyte. During the first charge, approximately ten electrons per molecule of **2** were passed, corresponding to the conversion of **2** to **1** (eight-electron process, Figure 4A) and then **1** to **1−KH** (two-electron process). Subsequent GCD cycles show a reversible capacity of ca. 210 mAh g^{-1} at a cell voltage of 1.3 V, consistent with in situ formation of electro-active **1** (Figure S12). ^{1}H and ^{13}C NMR analysis of the electrode materials (Figures S7 and S8) further confirms the complete conversion of **2** to **1**.

Next, we scaled up the electrochemical reduction of **2** to **1** to a two-gram scale. Bulk electrolysis was performed with a three-electrode setup using the standard alkaline electrolyte, a carbon counter electrode, and a Hg/HgO reference electrode. The conversion of **2** to **1** was 98% based on ^{1}H NMR analysis (Figure S9, top trace), affording an electrode of **1** with a 70:25:5 ratio with 11.1 mg cm^{-2} active material loading. The electrochemically generated electrode of **1** was cut and used directly in a coin cell. As expected, increasing the areal loading of active material (ca. 1 mg cm^{-2} to 11.1 mg cm^{-2}) reduces the rate capability. However, the overall performance maintains a capacity output similar to that of the smaller areal loading cells (Figures S14−S16).

To further demonstrate the viability of **1** in energy storage application,[49] we assembled a full cell with 11.1 mg cm^{-2} of active material loading and an anode: cathode mass ratio of 1:2. The anode of **1** was produced from in situ electrochemical reduction of **2.** The GCD of the full cells is comparable to that of the previously assessed half-cells (Figure 4B), except slightly increased voltage hysteresis (145 mV to 280 mV) after 1000 cycles. The high-loading full cell of Ni(OH)$_2$/**1** cells maintains 80% capacity after 812 cycles (Figures 4C and S17). By comparison, reports of Ni(OH)$_2$/Zn cells in a similar electrolyte of 4 M KOH + 2 M K_2CO_3 + 2 M KF (ZnO was added for stability of Zn anode) exhibit a faster decay to 80% capacity (425−460 cycles).[50] This comparative full-cell study supports the higher stability of **1** over inorganic anodes. Furthermore, compound **1** exhibits high voltage and specific capacity compared to other top-performing organic anode materials for alkaline batteries.[19,20,51−54] A detailed comparison can be found in Table S2. The specific energy of the full cell is 67 Wh kg^{-1}, including masses of the anode and the cathode, which is comparable to that of commercial NiMH batteries.[55]

In summary, we describe the electrochemical performance of benzo[c]cinnoline **1** as anode in AAB. Compared to conventional metal hydride anodes, **1** exhibits a similar capacity and voltage profile but higher stability. The reduced rate of HER at the organic electrode reduces self-discharge, provides additional stability, and enhances safety. We developed an in situ method for the formation of **1** ($100/g) from inexpensive **2** ($1.6/g) in high loading (11.1 mg

https://doi.org/10.1021/acsenergylett.4c03087
ACS Energy Lett. 2025, 10, 629−634

cm^{-2}) and adapted it into a full cell with a specific energy of 67 Wh kg^{-1}, which is comparable to most inorganic anodes used in AABs. Future works will investigate how the molecular structure of benzo[c]cinnoline (withdrawing groups, donating groups, extending the aromatic system, etc.) affects the redox mechanism and cycling performance.

■ ASSOCIATED CONTENT

Supporting Information

The Supporting Information is available free of charge at https://pubs.acs.org/doi/10.1021/acsenergylett.4c03087.

Additional experimental procedures, synthesis, and characterization method. Spectroscopic/electrochemical data (Figures S1−S18 and Tables S1−S2) (PDF)

■ AUTHOR INFORMATION

Corresponding Author

Shiyu Zhang − *Department of Chemistry and Biochemistry, The Ohio State University, Columbus, Ohio 43210, United States;* orcid.org/0000-0002-2536-4324; Email: zhang.8941@osu.edu

Authors

Christopher Walter − *Department of Chemistry and Biochemistry, The Ohio State University, Columbus, Ohio 43210, United States*

Jaehyun Park − *Department of Chemistry and Biochemistry, The Ohio State University, Columbus, Ohio 43210, United States*

Edgar U. Lopez-Torres − *Department of Chemistry and Biochemistry, The Ohio State University, Columbus, Ohio 43210, United States*

Mark Yaseen − *Department of Chemistry and Biochemistry, The Ohio State University, Columbus, Ohio 43210, United States*

Complete contact information is available at: https://pubs.acs.org/10.1021/acsenergylett.4c03087

Author Contributions

‡(C.W. and J.P.) These authors contributed equally.

Notes

The authors declare no competing financial interest.

■ ACKNOWLEDGMENTS

This work was supported by the National Science Foundation under CBET-2124604, the Sustainability Institute at Ohio State University, and the Center for Emergent Materials, NSF MRSEC, under award number DMR-2011876. The authors would like to thank the Turro laboratory (OSU), for sharing a sample of benzo[c]cinnoline, and Dr. Khalifa for the XPS analysis.

■ REFERENCES

(1) Jiang, L.; Hu, Y. C.; Ai, F.; Liang, Z.; Lu, Y. C. Rational Design of Anti-Freezing Electrolyte Concentrations via Freeze Concentration Process. *Energy Environ. Sci.* **2024**, *17* (8), 2815−2824.

(2) Jiang, L.; Lu, Y.; Zhao, C.; Liu, L.; Zhang, J.; Zhang, Q.; Shen, X.; Zhao, J.; Yu, X.; Li, H.; Huang, X.; Chen, L.; Hu, Y. S. Building Aqueous K-Ion Batteries for Energy Storage. *Nat. Energy* **2019**, *4* (6), 495−503.

(3) Liang, Y.; Yao, Y. Designing Modern Aqueous Batteries. *Nat. Rev. Mater.* **2023**, *8* (2), 109−122.

(4) Zhao, X.; Ma, L.; Shen, X. Co-Based Anode Materials for Alkaline Rechargeable Ni/Co Batteries: A Review. *J. Mater. Chem.* **2012**, *22* (2), 277−285.

(5) Luo, H.; Liu, B.; Yang, Z.; Wan, Y.; Zhong, C. The Trade-Offs in the Design of Reversible Zinc Anodes for Secondary Alkaline Batteries. *Electrochem. Energy Rev.* **2022**, *5* (1), 187−210.

(6) Shang, W.; Yu, W.; Liu, Y.; Li, R.; Dai, Y.; Cheng, C.; Tan, P.; Ni, M. Rechargeable Alkaline Zinc Batteries: Progress and Challenges. *Energy Storage Mater.* **2020**, *31* (June), 44−57.

(7) Olivetti, E. A.; Ceder, G.; Gaustad, G. G.; Fu, X. Lithium-Ion Battery Supply Chain Considerations: Analysis of Potential Bottlenecks in Critical Metals. *Joule* **2017**, *1* (2), 229−243.

(8) Feng, F.; Northwood, D. O. Self-Discharge Characteristics of a Metal Hydride Electrode for Ni-MH Rechargeable Batteries. *Int. J. Hydrogen Energy* **2005**, *30* (12), 1367−1370.

(9) Wang, C.; Marrero-Rivera, M.; Serafini, D. A.; Baricuatro, J. H.; Soriaga, M. P.; Srinivasan, S. The Self-Discharge Mechanism of AB5-Type Hydride Electrodes in Ni/MH Batteries. *Int. J. Hydrogen Energy* **2006**, *31* (5), 603−611.

(10) Lu, Y.; Zhang, Q.; Li, L.; Niu, Z.; Chen, J. Design Strategies toward Enhancing the Performance of Organic Electrode Materials in Metal-Ion Batteries. *Chem.* **2018**, *4* (12), 2786−2813.

(11) Huang, J.; Dong, X.; Guo, Z.; Wang, Y. Progress of Organic Electrodes in Aqueous Electrolyte for Energy Storage and Conversion. *Angew. Chem., Int. Ed.* **2020**, *59* (42), 18322−18333.

(12) Shi, M.; Das, P.; Wu, Z.; Liu, T.; Zhang, X. Aqueous Organic Batteries Using the Proton as a Charge Carrier. *Adv. Mater.* **2023**, *35* (42), 202302199.

(13) Zheng, Y.; Jiao, Y.; Zhu, Y.; Li, L. H.; Han, Y.; Chen, Y.; Du, A.; Jaroniec, M.; Qiao, S. Z. Hydrogen Evolution by a Metal-Free Electrocatalyst. *Nat. Commun.* **2014**, *5*, 2−9.

(14) Guo, X.; Apostol, P.; Zhou, X.; Wang, J.; Lin, X.; Rambabu, D.; Du, M.; Er, S.; Vlad, A. Towards the 4 V-Class n-Type Organic Lithium-Ion Positive Electrode Materials: The Case of Conjugated Triflimides and Cyanamides. *Energy Environ. Sci.* **2024**, *17* (1), 173−182.

(15) Wang, J.; Lakraychi, A. E.; Liu, X.; Sieuw, L.; Morari, C.; Poizot, P.; Vlad, A. Conjugated Sulfonamides as a Class of Organic Lithium-Ion Positive Electrodes. *Nat. Mater.* **2021**, *20* (5), 665−673.

(16) Dong, H.; Tutusaus, O.; Liang, Y.; Zhang, Y.; Lebens-Higgins, Z.; Yang, W.; Mohtadi, R.; Yao, Y. High-Power Mg Batteries Enabled by Heterogeneous Enolization Redox Chemistry and Weakly Coordinating Electrolytes. *Nat. Energy* **2020**, *5* (12), 1043−1050.

(17) Chen, T.; Banda, H.; Wang, J.; Oppenheim, J. J.; Franceschi, A.; Dincă, M. A Layered Organic Cathode for High-Energy, Fast-Charging, and Long-Lasting Li-Ion Batteries. *ACS Cent. Sci.* **2024**, *10* (3), 569−578.

(18) Li, L.; Chen, L.; Wen, Y.; Xiong, T.; Xu, H.; Zhang, W.; Cao, G.; Yang, Y.; Mai, L.; Zhang, H. Phenazine Anodes for Ultralongcycle-Life Aqueous Rechargeable Batteries. *J. Mater. Chem. A* **2020**, *8* (48), 26013−26022.

(19) Cui, H.; Zhang, D.; Wu, Z.; Zhu, J.; Li, P.; Li, C.; Hou, Y.; Zhang, R.; Wang, X.; Jin, X.; Bai, S.; Zhi, C. Tailoring Hydroxyl Groups of Organic Phenazine Anodes for High-Performance and Stable Alkaline Batteries. *Energy Environ. Sci.* **2024**, *17* (1), 114−122.

(20) Grieco, R.; Molina, A.; Sanchez, J. S.; Patil, N.; Liras, M.; Marcilla, R. A Significantly Improved Polymer||Ni(OH)2 Alkaline Rechargeable Battery Using Anthraquinone-Based Conjugated Microporous Polymer Anode. *Mater. Today Energy* **2022**, *27*, No. 101014.

(21) Zheng, Y.; Yu, D.; Wang, J.; Yang, J.; Luo, W.; Ge, T.; Qin, L.; Huang, Y.; Chen, D. A Phenazine-Derived Organic Anode for Ultrafast and Long-Life Aqueous Potassium-Ion Full Cells. *Sci. China Mater.* **2024**, *67* (5), 1464−1470.

(22) Choi, W.; Harada, D.; Oyaizu, K.; Nishide, H. Aqueous Electrochemistry of Poly(Vinylanthraquinone) for Anode-Active Materials in High-Density and Rechargeable Polymer/Air Batteries. *J. Am. Chem. Soc.* **2011**, *133* (49), 19839−19843.

(23) Zhang, X.; Zhang, X.; Miao, Y.; Huang, Q.; Chen, Z.; Guo, D.; Xu, J.; Shen, Y. M.; Cao, J. A Rechargeable Aqueous Phenazine-

Prussian Blue Proton Battery with Long Cycle Life. *J. Mater. Chem. A* **2023**, *11* (13), 7152−7158.
(24) Seçken, N.; Aksu, M. L.; Solak, A. O.; Kiliç, E. Electrochemical Behavior of Benzo[c]Cinnoline and Its Bromo Derivatives. *Turkish J. Chem.* **2002**, *26* (4), 617−626.
(25) Öztürk, F.; Durmuş, Z.; Uçkan, Ö. Ö.; Kiliç, E.; Kiliç, E. Synthesis and Electroreduction of 2-[(8-Hydroxyquinoline-5-Yl)-Azo]Benzo[c] Cinnoline in Dmso-H2O (1:1) Medium. *Collect. Czechoslov. Chem. Commun.* **2010**, *75* (11), 1201−1216.
(26) Durmuş, Z.; Solak, A. O.; Durmuş, S.; Kiliç, E. Electrochemical Behaviour of 3,8-Difluorobenzo[c]Cinnoline at Mercury Electrode. *Talanta* **2001**, *55* (2), 357−362.
(27) Millefiori, S. Effects of Proton Donors on the Electrochemical Reduction of Benzo[c]Cinnoline in Acetonitrile. *J. Heterocycl. Chem.* **1980**, *17* (7), 1541−1543.
(28) Huang, J.; Cao, Y.; Cao, M.; Zhong, J. Improving the Capacity of Zinc-Ion Batteries through Composite Defect Engineering. *RSC Adv.* **2021**, *11* (54), 34079−34085.
(29) Liu, J.; Wang, J.; Xu, C.; Jiang, H.; Li, C.; Zhang, L.; Lin, J.; Shen, Z. X. Advanced Energy Storage Devices: Basic Principles, Analytical Methods, and Rational Materials Design. *Adv. Sci.* **2018**, *5* (1), 1700322.
(30) Nikolic, M.; Cesarini, A.; Billeter, E.; Weyand, F.; Trtik, P.; Strobl, M.; Borgschulte, A. Hydrogen Transport and Evolution in Ni-MH Batteries by Neutron Imaging. *Angew. Chem., Int. Ed.* **2023**, *62* (45), No. e202307367.
(31) Notten, P. H. L. Rechargeable Nickel-Metalhydride Batteries: A Successful New Concept. In *Interstitial intermetallic alloys*; Springer, 1995; pp 151−195 DOI: 10.1007/978-94-011-0295-7_7.
(32) Notten, P. H. L.; Latroche, M. Secondary Batteries-Nickel Systems: Nickel−Metal Hydride: Metal Hydrides: Metal Hydrides. In *Encyclopedia of electrochemical power sources*; Elsevier, 2009; pp 502−521 DOI: 10.1016/B978-044452745-5.00164-7.
(33) Yang, T. H.; Pyun, S. Il. Hydrogen Transport through LaNi4.7Al0.3Hx Porous Electrode in the Coexistence of Two Hydride Phases (α- and β-Phases): Current Transient Analysis. *Electrochim. Acta* **1998**, *43* (5−6), 471−478.
(34) Yuan, X.; Xu, N. Determination of Hydrogen Diffusion Coefficient in Metal Hydride Electrode by Cyclic Voltammetry. *J. Alloys Compd.* **2001**, *316* (1−2), 113−117.
(35) Hausmann, J. N.; Traynor, B.; Myers, R. J.; Driess, M.; Menezes, P. W. The PH of Aqueous NaOH/KOH Solutions: A Critical and Non-Trivial Parameter for Electrocatalysis. *ACS Energy Lett.* **2021**, *6* (10), 3567−3571.
(36) Alván, D.; Grieco, R.; Patil, N.; Mavrandonakis, A.; Liras, M.; Marcilla, R. Hybrid Based on Phenazine Conjugated Microporous Polymer as a High-Performance Organic Electrode in Aqueous Electrolytes. *Batter. Supercaps* **2023**, *6* (5), No. e202300023.
(37) Minsky, A.; Cohen, Y.; Rabinovitz, M. Novel Polycyclic Dianions: Metal Reduction of Nitrogen Heterocycles. *J. Am. Chem. Soc.* **1985**, *107* (6), 1501−1505.
(38) Stone, I. B.; Jermaks, J.; MacMillan, S. N.; Lambert, T. H. The Hydrazine−O2 Redox Couple as a Platform for Organocatalytic Oxidation: Benzo[c]Cinnoline-Catalyzed Oxidation of Alkyl Halides to Aldehydes. *Angew. Chem., Int. Ed.* **2018**, *57* (38), 12494−12498.
(39) Isbir-Turan, A. A.; Üstündağ, Z.; Kiliç, E.; Güzel, R.; Uçkan, Ö.; Solak, A. O. 2-Benzo[c]Cinnoline and 2-Benzo[c]Cinnoline 6-Oxide Modified Glassy Carbon Electrodes: Electrocatalytic Reduction of Dioxygen in Aqueous Media. *Instrum. Sci. Technol.* **2011**, *39* (2), 149−160.
(40) Goswami, A.; Koskey, S.; Mukherjee, T.; Chyan, O. Study of Pyrazole as Copper Corrosion Inhibitor in Alkaline Post Chemical Mechanical Polishing Cleaning Solution. *ECS J. Solid State Sci. Technol.* **2014**, *3* (10), P293−P297.
(41) Katrib, A.; El-Rayyes, N. R.; Al-Kharafi, F. M. N 1s Orbital Binding Energies of Some Pyrazole Pyrazoline Compounds by XPS. *J. Electron Spectrosc. Relat. Phenom.* **1983**, *31* (3), 317−321.
(42) Kiernicki, J. J.; Higgins, R. F.; Kraft, S. J.; Zeller, M.; Shores, M. P.; Bart, S. C. Elucidating the Mechanism of Uranium Mediated Diazene N = N Bond Cleavage. *Inorg. Chem.* **2016**, *55* (22), 11854−11866.
(43) Dehghanpour, S.; Afshariazar, F.; Assoud, J. Reduction of 2,2′-Dinitrobiphenyl with Hydrazine Hydrate Catalyzed by Pd/C: Cobalt(II), Zinc(II) and Mercury(II) Complexes with Benzo[c]-Cinnoline and N 2,N 2′-Bis(3-Phenylallylidene)Biphenyl-2,2′-Diamine. *Polyhedron* **2012**, *35* (1), 69−76.
(44) Moore, R. E.; Furst, A. Reductions with Hydrazine Hydrate Catalyzed by Raney Nickel. III. Effect of the Catalyst on the Reduction of 2,2′-Dinitrobiphenyl. *J. Org. Chem.* **1958**, *23* (10), 1504−1506.
(45) Wada, S.; Urano, M.; Suzuki, H. The Newborn Surface of Dull Metals in Organic Synthesis. Bismuth-Mediated Solvent-Free One-Step Conversion of Nitroarenes to Azoxy- and Azoarenes. *J. Org. Chem.* **2002**, *67* (23), 8254−8257.
(46) Meng, R.; Li, F.; Li, D.; Jin, B. A Green and Efficient Synthesis Method of Benzo[c]Cinnolines: Electrochemical Reduction of 2,2'-Dinitrobiphenyl in the Presence of CO 2. *ChemElectroChem.* **2022**, *9* (5), No. e202101381.
(47) Ma, Y.; Wu, S.; Jiang, S.; Xiao, F.; Deng, G. J. Electrosynthesis of Azobenzenes Directly from Nitrobenzenes. *Chin. J. Chem.* **2021**, *39* (12), 3334−3338.
(48) Chang, L.; Li, J.; Wu, N.; Cheng, X. Chemoselective Electrochemical Reduction of Nitroarenes with Gaseous Ammonia. *Org. Biomol. Chem.* **2021**, *19* (11), 2468−2472.
(49) Brisse, A. L.; Stevens, P.; Toussaint, G.; Crosnier, O.; Brousse, T. Ni(OH)2 and NiO Based Composites: Battery Type Electrode Materials for Hybrid Supercapacitor Devices. *Materials (Basel).* **2018**, *11* (7), 1178.
(50) Adler, T. C.; McLarnon, F. R.; Cairns, E. J. Investigations of a New Family of Alkaline-Fluoride-Carbonate Electrolytes for Zinc/Nickel Oxide Cells. *Ind. Eng. Chem. Res.* **1998**, *37* (8), 3237−3241.
(51) Liu, X.; Ni, Y.; Yang, Z.; Lu, Y.; Xie, W.; Yan, Z.; Chen, J. Ampere-Hour-Scale Aqueous Nickel−Organic Batteries Based on Phenazine Anode. *Adv. Energy Mater.* **2024**, 2403628.
(52) Liang, Y.; Jing, Y.; Gheytani, S.; Lee, K. Y.; Liu, P.; Facchetti, A.; Yao, Y. Universal Quinone Electrodes for Long Cycle Life Aqueous Rechargeable Batteries. *Nat. Mater.* **2017**, *16* (8), 841−848.
(53) Li, Y.; Liu, L.; Liu, C.; Lu, Y.; Shi, R.; Li, F.; Chen, J. Rechargeable Aqueous Polymer-Air Batteries Based on Polyanthraquinone Anode. *Chem.* **2019**, *5* (8), 2159−2170.
(54) Dražević, E.; Andersen, A. S.; Wedege, K.; Henriksen, M. L.; Hinge, M.; Bentien, A. Investigation of Low-Cost Oligoanthraquinones for Alkaline, Aqueous Rechargeable Batteries with Cell Potential up to 1.13 V. *J. Power Sources* **2018**, *381* (Feb), 94−100.
(55) Ash, B.; Nalajala, V.; Popuri, A.; Subbaiah, T.; Minakshi, M. Perspectives on Nickel Hydroxide Electrodes Suitable for Rechargeable Batteries: Electrolytic vs. Chemical Synthesis Routes. *Nanomaterials* **2020**, *10* (9), 1878.

https://doi.org/10.1021/acsenergylett.4c03087
ACS Energy Lett. 2025, 10, 629−634